PONTIFICIA UNIVERSIDAD CATOLICA DE CHILE
SCHOOL OF ENGINEERING

APPLICATION OF THE FRACTIONAL FOURIER TRANSFORM TO IMAGE RECONSTRUCTION IN MRI

VICENTE JOSÉ PAROT FERNÁNDEZ

Thesis submitted to the Office of Research and Graduate Studies
in partial fulfillment of the requirements for the degree of
Master of Science in Engineering

Advisor:
PABLO IRARRÁZAVAL M.

Santiago de Chile, December 2009

PONTIFICIA UNIVERSIDAD CATOLICA DE CHILE
SCHOOL OF ENGINEERING

APPLICATION OF THE FRACTIONAL FOURIER TRANSFORM TO IMAGE RECONSTRUCTION IN MRI

VICENTE JOSÉ PAROT FERNÁNDEZ

Members of the Committee:
PABLO IRARRÁZAVAL M.
CRISTIÁN TEJOS N.
CARLOS LIZAMA Y.
JORGE VERA A.

Thesis submitted to the Office of Research and Graduate Studies
in partial fulfillment of the requirements for the degree of
Master of Science in Engineering

Santiago de Chile, December 2009

To my parents Sarita and Sergio

ACKNOWLEDGEMENTS

First of all, nothing of what I have done could have been possible without the great opportunities I have had, for which I would like to thank God and my parents, Sergio and Sarita. They have been the first to encourage me to continue my work permanently and a very good motivation.

Among the many people I would like to thank, the best is my girlfriend Cote Achurra, who has been a constant support and inspiration not only in my work but also in all other aspects of my life.

In other aspects, the brilliant team which I have worked with during my time as a student at the Biomedical Imaging Center deserves much gratitude, I would like to thank Cristián Tejos, Carlos Sing-Long, Carlos Lizama, Sergio Uribe, Cristóbal Arrieta, Caro Arboleda, Claudia Prieto and all other past members I have met. Their contribution has been very important with the good ideas we have discussed, with their valuable suggestions and also with their human values, humor and company. I would like to give special thanks to its director Pablo Irarrázaval, my thesis advisor, whom I have get to know as a teacher, a researcher and a person, with his passion and motivation he has been a clear example of how to devote to something.

I need to refer to all who have been my teachers, all that I have learned from them has contributed to the finalization of my thesis and my studies. Together with some members of my family as Julio, Eduardo and Pablo, they have also increased my interest in learning with their motivation and example, for which I am also very grateful.

I also thank my close friends and all people who have supported me and have been available to serve as volunteers and to hear about my thesis despite their possible lack of understanding.

TABLE OF CONTENTS

LIST OF FIGURES

ABSTRACT

To obtain good quality images with Magnetic Resonance (MR) it is necessary to have good spatial homogeneity in the B_0 field for the region of imaging. Field homogeneity is difficult to achieve, particularly for short bore magnets and higher fields. When the passive or active shimming are not enough, or when the inhomogeneity comes from differences in susceptibility between adjacent regions within an object, there are several post-processing techniques for correcting the distortions. These techniques do not have a well supported theoretical background with the exception of linear terms. We propose to use the Fractional Fourier Transform (FrFT) for reconstructing the MR signal acquired under the presence of quadratic fields. The FrFT provides a precise theoretical framework for this. In this work we show how the FrFT can be used to understand the distortions and to reconstruct MR data acquired under that condition. We also show examples of reconstruction for simulated and volunteer data under quadratic inhomogeneities obtaining an improved image quality compared with standard Fourier reconstructions. The FrFT opens a new paradigm for understanding and correcting second degree off-resonances with the potential for manufacturing shorter magnets.

Keywords: fractional Fourier transform, magnetic resonance imaging, MRI, image reconstruction, field inhomogeneities, off–resonance correction.

RESUMEN

Para obtener Imágenes de Resonancia Magnética (MRI) de buena calidad, es necesario tener una buena homogeneidad espacial en el campo B_0 de la región a observar. La homogeneidad de campo es difícil de lograr, particularmente para imanes de núcleo corto y campos altos. Cuando el ajuste fino pasivo o activo no es suficiente, o cuando la inhomogeneidad viene de diferencias en la susceptibilidad entre regiones adyacentes dentro de un objeto, hay varias técnicas de post–procesamiento para corregir las distorsiones. Éstas técnicas no tienen un fundamento teórico sólido con la excepción de las relativas a términos lineales. Proponemos usar la Transformada Fraccionaria de Fourier (FrFT) para reconstruir señales MRI obtenidas en campos con desviaciones cuadráticas. La FrFT provee un marco teórico preciso para esto. En este trabajo mostramos cómo se puede usar la FrFT para entender las distorsiones y reconstruir señales MRI que han sido obtenidas en campos con inhomogeneidad cuadrática. Mostramos además ejemplos de reconstrucción de datos simulados y datos de voluntarios con inhomogeneidades cuadráticas, obteniéndose una mejor calidad de imagen que al usar reconstrucción estándar de Fourier. La FrFT abre un nuevo paradigma para entender y corregir distorsiones de fuera de resonancia con el potencial de fabricar imanes más cortos.

Palabras Claves: transformada fraccionaria de Fourier, imágenes de resonancia magnética, MRI, reconstrucción de imágenes, inhomogeneidades de campo, corrección de inhomogeneidades de fuera de resonancia.

1. INTRODUCTION

Magnetic Resonance (MR) imaging and spectroscopy provide a number of practical applications for both clinical and scientific purposes (Liang & Lauterbur, 2000; Kalinowski, Berger, & Braun, 1988). For this technique it is necessary to have a strong magnetic field with uniform intensity across the entire field of view. However, deviations from the constant magnetic field are inherent to MR systems as uniform fields are physically difficult to achieve and as adjacent regions within the scanned object show different susceptibilities, producing inhomogeneities. Such field variations introduce an accumulating phase over time into the MR signal, which cannot be demodulated easily as it varies spatially. This problem is worse when stronger uniform fields are considered and whenever sequences with long acquisition time are used. High field MR system designs have to observe this limitation, sometimes using secondary coils to correct the field, simply reducing the entire measurement volume or using a local region of interest for each measurement (Vedrine, 2008; Vaughan et al., 2006). Passive and active shimming techniques help reducing inhomogeneities and are commonly used, partially correcting first and second order field variations in most cases.

Several image reconstruction methods have been proposed to correct distortions produced by non homogeneous fields, being an active field of research (Akel, Rosenblitt, & Irarrazaval, 2002; Chen & Meyer, 2008; Chen, Sica, & Meyer, 2008; Fessler, Lee, Olafsson, Shi, & Noll, 2005; Irarrazabal, Meyer, Nishimura, & Macovski, 1996; Manjón et al., 2007; Noll, Fessler, & Sutton, 2005; Sutton, Noll, & Fessler, 2003; Vovk, Pernus, & Likar, 2004). There is a well known theory background for the linear correction approaches, in which an exact analytical solution is provided (Akel et al., 2002; Irarrazabal et al., 1996), but both for second–order and arbitrary field maps there is no such conclusive theory background.

The Fractional Fourier Transform (FrFT) is a generalization of the standard Fourier Transform (FT) by means of the continuous fractional order a, which covers densely the entire transition between image (or time) domain ($a = 0$) and the Fourier domain ($a = 1$)

(Ozaktas, Kutay, & Zalevsky, 2001). The FrFT can be defined in several different ways leading to different physical interpretations and thus, it has become useful in many applications (Ozaktas & Mendlovic, 1993, 1995; Yetik, 2001). It has been shown that the FT properties are special cases of FrFT properties (Ozaktas et al., 2001) and further research has been done in discretization (Candan, Kutay, & Ozaktas, 2000; Ozaktas & Sumbul, 2006), fast computation (Bultheel, 2004), and other aspects of the FrFT related to signal processing (Guven, Ozaktas, Cetin, & Barshan, 2008; Ozaktas, Barshan, Mendlovic, & Onural, 1994; Ozaktas, Arikan, Kutay, & Bozdagt, 1996; Ozaktas, Barshan, & Mendlovic, 1994).

It is of general knowledge that the magnetization of an object under a uniform magnetic field can be related to its FT. Similarly, we noted that the magnetization of an object under a quadratic magnetic field can be related to its FrFT. In fact, the defining integral kernel of the FT presents a correspondence with the MR signal generated by a magnetized object in a uniform magnetic field and thus, it allows reconstructing the object by taking an inverse FT of its MR signal. Equivalently, the kernel that provides the integral definition of the FrFT presents a clear resemblance with the MR signal generated by an object with an underlying quadratic magnetic field, i.e. a field which intensity varies spatially as a second order polynomial. This fact suggested us that there is a framework that allows native MR reconstruction from quadratic fields.

In this manuscript we present a theoretical description of the relationship between the FrFT and the MR signal generated when quadratic magnetic fields are used. Furthermore, we propose a general MR method based on the FrFT that allows the acquisition and reconstruction of MR signals of objects that have been obtained with quadratic fields.

In Chapter 2, we propose a new FrFT–based framework that allows fractional Fourier understanding of the MR signal obtained with quadratic field inhomogeneities, showing examples with simple trajectories. We explain the relationship between the FrFT and the MR signal in a one–dimensional context, which is extended to two dimensions in Chapter 3. We propose a general reconstruction method based on the FrFT in Chapter 4. In Chapter 5

we describe the experimental setup and methods, and in Chapter 6 we show the results of our simulation, phantom and *in–vivo* experiments. Chapter 7 includes further discussions and conclusions from this work and suggestions for future work.

2. THEORY

In this section we explain the relation between the Fractional Fourier Transform and an MR signal acquired under a quadratic main field, showing how the MR signal can be written as a FrFT. This framework allows us to analyze the acquired data in a fractional order polar space, from where we can extract visual insight.

2.1. Fractional Fourier Transform

The a–th order FrFT $f_a(\rho) = \mathcal{F}^a\{f\}(\rho)$ of the signal $f(u)$ for $0 < |a| < 2$ can be expressed as an integral transform as (taken from (Ozaktas et al., 2001) with a slight change of notation)

$$f_a(\rho) = C_\alpha(\rho) \int f(u)\, \mathrm{e}^{i\pi\left(u^2 \cot\alpha - 2\rho u \csc\alpha\right)}\, du \tag{2.1}$$

$$C_\alpha(\rho) \equiv \mathrm{e}^{i\pi\rho^2 \cot\alpha}\sqrt{1 - i\cot\alpha}, \quad \alpha \equiv a\pi/2 \tag{2.2}$$

Note that the most notable difference between this equation and the Fourier transform is an extra quadratic phase in the kernel.

Throughout this section, we have selected u and ρ to denote dimensionless variables in order to maintain formal consistency between the MRI and FrFT contexts. The independent variable ρ is the pseudo–frequency in any fractional domain and u is the particular case of ρ for the 0–th order (the object axis). The relation between the dimensionless u and its dimensional counterpart x will be addressed at the end of Chapter 4.

2.2. MRI Signal under quadratic field map inhomogeneity

At first, we will consider the single–dimensional case. Let $f(u)$ be the magnetization of the object of interest. The MRI signal, in a perfect uniform B_0 field, ignoring T_1 and T_2 relaxations and after demodulation at the Larmor frequency ω_0 is

$$s(t) = \int f(u)\, \mathrm{e}^{-i2\pi k(t)u}\, du$$

where, as customarily defined, $k(t) = \gamma/2\pi \int_0^t G(\xi)d\xi$ is the k–space trajectory.

Whenever there is an inhomogeneous field $B(u) = B_0 + p(u)$ as a function of space, the magnetization is modulated by a time–dependent phase. For the particular case of a quadratic inhomogeneity, $p(u) = p_2u^2 + p_1u + p_0$. In this case the signal equation becomes

$$s(t) = e^{-i2\pi p_0 t} \int f(u)\, \mathrm{e}^{i\pi\left(-2p_2tu^2 - 2(k(t)+p_1t)u\right)}\, du \tag{2.3}$$

There is a remarkable similarity between this expression and the FrFT defined in (2.1). Consequently, it is natural to think that the FrFT can be used to reconstruct this data. Moreover, the FrFT is a theoretical tool that could allow us to extend the framework of MRI to quadratic fields, while recovering the homogeneous–field case as a particular case.

2.3. Link between the MRI Signal and the FrFT

In order to represent (2.3) in the form of (2.1), we define

$$\begin{aligned} \alpha(t) &= \cot^{-1}(-2p_2t), \text{ and} \\ \rho(t) &= \frac{k(t) + p_1t}{\csc\alpha(t)} = \frac{k(t) + p_1t}{\sqrt{1 + 4p_2^2t^2}} \end{aligned} \tag{2.4}$$

In this definition, both α and ρ are functions of time but we will often omit this for the sake of simplicity. We use $\alpha \in (0, \pi)$, which ensures $\csc\alpha > 0$, and $\cot^{-1}$ being invertible. Therefore we can write the relations $-2p_2t = \cot\alpha$ and $-2\left(k(t) + p_1t\right) = -2\rho\csc\alpha$. With these variables the signal in (2.3) becomes

$$s(t) = \mathrm{e}^{-i2\pi p_0 t} \int f(u)\, \mathrm{e}^{i\pi\left(u^2\cot\alpha - 2\rho u\csc\alpha\right)}\, du$$

Using (2.1) we can express the signal equation as a time–varying order FrFT of the object

$$\begin{aligned} s(t) &= \mathrm{e}^{-i2\pi p_0 t} C_\alpha(\rho)^{-1} f_a(\rho) \\ f_a(\rho) &= \mathrm{e}^{i2\pi p_0 t} C_\alpha(\rho) s(t) \end{aligned} \tag{2.5}$$

Note that if α were constant and equal to $\pi/2$ (or $a = 1$), we recover the signal equation in terms of the standard Fourier transform.

The advantage of this relation is that we have a well known framework for working with quadratic terms in the magnetic field. In general, the inhomogeneity of the field will be better approximated by a second order polynomial. Additionally, second order terms naturally occur in coil design and are the most significant terms within second and upper orders.

2.4. The ρ–α space

The terms α and ρ in (2.4) define a parametric trajectory $(\rho(t), \alpha(t))$ in a space that we call ρ–α space. Since α is an angle, this space is conveniently represented in polar coordinates. The trajectory in ρ–α space starts immediately after the excitation ($t = 0$) in the frequency or Fourier direction ($\alpha = \pi/2$) and as time passes it curves toward the object axis ($\alpha = 0$).

In what follows we will analyze some common trajectories using this framework. For the sake of simplicity, we neglect the restrictions on the maximum slew rate.

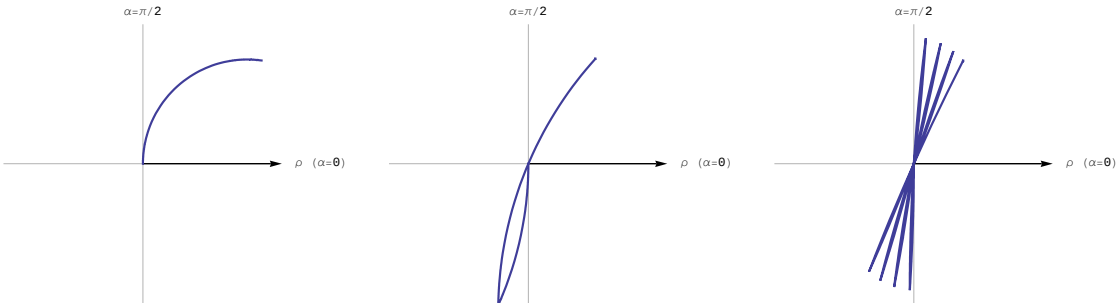

(a) (b) (c)

FIGURE 2.1. Examples of typical trajectories over a quadratic field in the polar representation of ρ–α space. (a) A constant gradient can be represented as a circular path. (b) A 2DFT bipolar gradient describes two circular arcs. (c) The polar graph shows the ρ–α space in the readout direction for seven readout echoes of an EPI trajectory.

2.4.1. Constant gradient

Let us assume that the readout gradient G_0 is constant and starts at $t = 0$, as would be the case in a projection reconstruction sequence. Assume also that the inhomogeneity

is purely quadratic $p(u) = p_2 u^2$. Linear and constant terms can be ignored without loss of generality, because the first is equivalent to a change in the amplitude of the gradient and the second can be corrected during the signal demodulation. Then $k(t)$ would be $\int_0^t G_0 d\tau = G_0 t$ and the trajectory in ρ–α space would be

$$\begin{aligned} \alpha(t) &= \cot^{-1}(-2p_2 t) \\ \rho(t) &= \frac{k(t) + p_1 t}{\sqrt{1 + 4p_2^2 t^2}} = \frac{G_0 t}{\sqrt{1 + 4p_2^2 t^2}} \end{aligned}$$

which is the parametric form of a circumference centered at $(G_0/4p_2, 0)$. Fig. 2.1 (a) shows this trajectory starting in $t = 0$ at the origin. Assuming $p_2 < 0$, which resembles the typical case in which the intensity of the B_0 field is greater at the center of a magnet, we also observe that the trajectory asymptotically approaches the object axis ($\alpha = 0$) as t increases.

As expected, for small values of t, the trajectory deviates little from the frequency axis ($\alpha = \pi/2$), and therefore distortions due to field variations are small. This is consistent with the general knowledge that short readouts are less sensitive to inhomogeneities.

We also note that if p_2 tends to zero, the field inhomogeneity vanishes and the center of the circumference located at $G_0/4p_2$ tends to infinity. Equivalently, the ρ–α trajectory becomes a straight line in the frequency direction

$$\begin{aligned} \alpha(t) &= \cot^{-1}(-2p_2 t) = \frac{\pi}{2} \\ \rho(t) &= \frac{G_0 t}{\sqrt{1 + 4p_2^2 t^2}} = G_0 t \end{aligned}$$

2.4.2. Standard 2DFT readout

Considering again that the field distortion is $p(u) = p_2 u^2$, we now assume that the gradient is formed by a negative pulse of duration t_0 followed by a positive one, as is

standard in 2DFT readouts. In this case

$$k(t) = \int_0^t G(\tau)d\tau = \begin{cases} -G_0 t & 0 < t < t_0 \\ G_0(t - 2t_0) & t_0 < t \end{cases}$$

Consequently, the trajectory in ρ–α space is given by

$$\begin{aligned} \alpha(t) &= \cot^{-1}(-2p_2 t) \\ \rho(t) &= \frac{1}{\sqrt{1 + 4p_2^2 t^2}} \times \begin{cases} -G_0 t & 0 < t < t_0 \\ G_0(t - 2t_0) & t_0 < t \end{cases} \end{aligned}$$

This trajectory is formed by two circular arcs. The trajectory describes one arc for the negative gradient centered at $(-G_0/4p_2, 0)$ and continues to the other one centered at $(G_0/4p_2, -G_0 t_0)$, which corresponds to the positive gradient, as shown in Fig. 2.1 (b).

2.4.3. EPI readout

If the gradient were a train of negative and positive pulses as is used in Echo Planar Imaging

$$G(t) = \begin{cases} -G_0 & \text{for } 0 < t < t_0,\ 3t_0 < t < 5t_0,\ ... \\ G_0 & \text{for } t_0 < t < 3t_0,\ 5t_0 < t < 7t_0,\ ... \end{cases}$$

the described ρ–α trajectory would be composed by a series of circular arcs centered at $(\pm G_0/4p_2, \mp jG_0 t_0/2)$, $j = 0, 1, 2, ...$ as shown in Fig. 2.1 (c).

2.4.4. Spectroscopy

If the sequence has no gradients, as in a pure spectroscopic acquisition, the trajectory will only depend on the linear term of the field deviation p_1

$$\begin{aligned} \alpha(t) &= \cot^{-1}(-2p_2 t) \\ \rho(t) &= \frac{k(t) + p_1 t}{\sqrt{1 + 4p_2^2 t^2}} = \frac{p_1 t}{\sqrt{1 + 4p_2^2 t^2}} \end{aligned}$$

and will have the shape shown in Fig. 2.1 (a), centered at $(p_1/4p_2, 0)$. If $p_1 = 0$, the trajectory is a singularity at the origin of the ρ–α space. In this case it is more convenient to represent the space in Cartesian coordinates (ρ, a), and the readout trajectory $\rho = 0$ becomes equivalent to acquire the continuous component of the FrFT for the orders a.

3. EXTENSION TO TWO DIMENSIONS

To extend the correspondence of the signal equation to the FrFT definition we employ the fact that the latter is separable and easily written in vector form. In two dimensions the FrFT is (Ozaktas et al., 2001)

$$f_{\mathbf{a}}(\boldsymbol{\rho}) = C_{\boldsymbol{\alpha}}(\boldsymbol{\rho}) \int f(\mathbf{u})\, \mathrm{e}^{i\pi(\mathbf{u}^{\mathrm{T}}\mathbf{A}\mathbf{u} - 2\mathbf{u}^{\mathrm{T}}\mathbf{B}\boldsymbol{\rho})} d\boldsymbol{u}$$

with

$$\mathbf{u} = \begin{bmatrix} u \\ v \end{bmatrix},\ \boldsymbol{\rho} = \begin{bmatrix} \rho_u \\ \rho_v \end{bmatrix},\ \mathbf{a} = \begin{bmatrix} a_u \\ a_v \end{bmatrix},\ \boldsymbol{\alpha} = \mathbf{a}\frac{\pi}{2} = \begin{bmatrix} \alpha_u \\ \alpha_v \end{bmatrix}$$

$$\mathbf{A} = \begin{bmatrix} \cot\alpha_u & 0 \\ 0 & \cot\alpha_v \end{bmatrix},\ \mathbf{B} = \begin{bmatrix} \csc\alpha_u & 0 \\ 0 & \csc\alpha_v \end{bmatrix}$$

and $C_{\boldsymbol{\alpha}}(\boldsymbol{\rho}) = \sqrt{1 - i\cot\alpha_u}\sqrt{1 - i\cot\alpha_v}\, \mathrm{e}^{i\pi\boldsymbol{\rho}^T \boldsymbol{A}\boldsymbol{\rho}}$.

To write the signal equation in 2D we write the field distortion as $p(\mathbf{u}) = \mathbf{u}^{\mathrm{T}}\mathbf{p}_2\mathbf{u} + \mathbf{u}^{\mathrm{T}}\mathbf{p}_1 + p_0$, with

$$\mathbf{p}_1 = \begin{bmatrix} p_{1u} \\ p_{1v} \end{bmatrix} \text{ and } \mathbf{p}_2 = \begin{bmatrix} p_{2u} & 0 \\ 0 & p_{2v} \end{bmatrix}$$

so that it becomes

$$s(t) = \mathrm{e}^{-i2\pi p_0 t} \int f(\mathbf{u})\, \mathrm{e}^{i\pi(-2\mathbf{u}^{\mathrm{T}}\mathbf{p}_2\mathbf{u}t - 2\mathbf{u}^{\mathrm{T}}(\mathbf{k}(t) + \mathbf{p}_1 t))} d\mathbf{u} \tag{3.1}$$

with $\mathbf{k}(t) = [k_u(t)\ \ k_v(t)]^{\mathrm{T}}$. Note that we also assumed that the field distortion is diagonal in the coordinate axis, i.e. the terms outside the diagonal of $\mathbf{p}_2$ are zero in order to match the separable form of the FrFT.

Remark that both $\mathbf{A}$ and $\mathbf{B}$ are diagonal matrices that depend on $\boldsymbol{\alpha}$. We can proceed as we did previously to define the four–dimensional ρ–α space using the change of variables:

$$\begin{aligned}
\cot \alpha_u &= -2p_{2u}t \\
\cot \alpha_v &= -2p_{2v}t \\
\rho_u \csc \alpha_u &= k_u(t) + p_{1u}t \\
\rho_v \csc \alpha_v &= k_v(t) + p_{1v}t
\end{aligned}$$

which is equivalent to solve for $\boldsymbol{\alpha}$ and $\boldsymbol{\rho}$ the matrix equations $\boldsymbol{A}(\boldsymbol{\alpha}) = -2\boldsymbol{p}_2 t$ and $\boldsymbol{B}(\boldsymbol{\alpha})\boldsymbol{\rho} = \boldsymbol{k}(t) + \boldsymbol{p}_1 t$. Finally, the signal equation can be expressed in terms of a 2D varying–order FrFT as

$$s(t) = \mathrm{e}^{-i2\pi p_0 t} C_{\boldsymbol{\alpha}}(\boldsymbol{\rho})^{-1} f_{\mathbf{a}}(\boldsymbol{\rho})$$

4. RECONSTRUCTION

In the FrFT framework, the reconstruction problem requires to know both the pseudo–frequency and the transform order where the data was acquired. These can be determined using (2.4). The object will be the solution to the inverse of (2.5) (ignoring the constant field deviation p_0)

$$\begin{aligned}\hat{f}(u) &= \mathcal{F}^{-a}\left\{f_{a(t)}\left(\rho(t)\right)\right\}(u) \\ &= \mathcal{F}^{-a}\left\{C_{\alpha(t)}\left(\rho(t)\right)s(t)\right\}(u)\end{aligned}$$

In this expression we have made explicit the time dependence of α. This dependency implies that the fractional order changes with time and therefore a inverse FrFT is not feasible. We analyze three different reconstruction approaches: standard inverse Fourier reconstruction; inverse fractional Fourier reconstruction; and variable order inverse fractional Fourier reconstruction. The difference between these reconstructions is the assumption they make on where the data is placed in the ρ–α space. In Fig. 4.1 we show the actual ρ–α space trajectory and the assumption of the reconstruction scheme for a standard 2DFT readout.

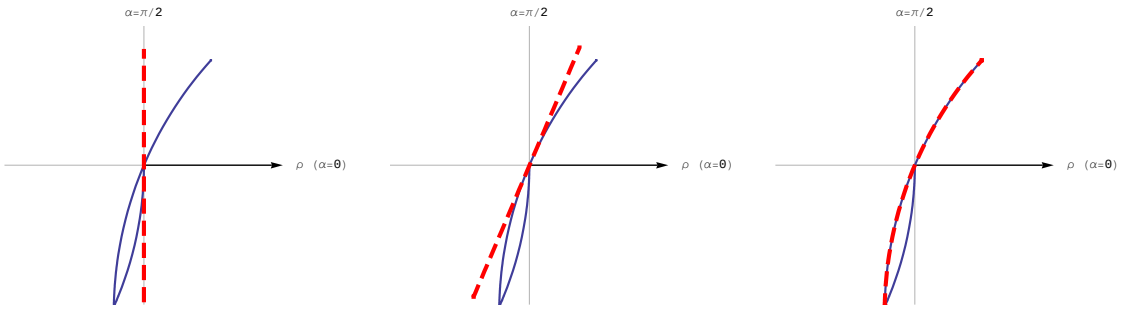

(a) (b) (c)

FIGURE 4.1. Example of a one dimensional 2DFT trajectory in the polar representation of ρ–α space represented by the continuous line and its reconstruction interpretation represented by the dashed line. (a) Standard Fourier interpretation. (b) Fractional Fourier interpretation. (c) Variable order inverse fractional Fourier interpretation.

4.1. Standard Inverse Fourier Reconstruction

The first approach is to perform the reconstruction by using the standard inverse Fourier transform. This is equivalent to assume that $\alpha \equiv \pi/2$, $\cot\alpha \equiv 0$ and $C_{\pi/2}(\rho) \equiv 1$. The reconstructed object is

$$\hat{f}_1(u) = \mathcal{F}^{-1}\left\{s(t)\right\}(u)$$

The samples are acquired in the curved trajectory but are interpreted as being in the frequency axis (vertical dashed line of Fig. 4.1(a)). The distortions in the image will depend on how much the reconstruction locations differ from the sampling locations.

4.2. Inverse Fractional Fourier Reconstruction

The second approach is to assume that the samples are being acquired at a constant order, which can be though as a tangent approximation in the ρ–α plane. This approach has two advantages: (i) the reconstruction and sampling locations are closer; and (ii) the inverse expression is exactly a inverse FrFT

$$\hat{f}_{\bar{a}}(u) = \mathcal{F}^{-\bar{a}}\left\{C_{\bar{\alpha}}\left(\rho(t)\right)s(t)\right\}(u)$$

where $\bar{a}$ (or $\bar{\alpha}$) is the order (or angle for the tangent line) at the origin. As we will show in Chapter 6, this reconstruction provides a better approximation to the real object since it improves the accuracy of the reconstructed phase over the standard Fourier reconstruction. However, the magnitude is the same as the one obtained with the standard Fourier reconstruction. Using the definitions in (2.1) and (2.2) it can be seen that

$$\hat{f}_{\bar{a}}(u) = \mathrm{e}^{-i\pi u^2\cot\bar{\alpha}}|\csc\bar{\alpha}|\int s(t)\,\mathrm{e}^{i2\pi u\rho\csc\bar{\alpha}}\,d\rho \tag{4.1}$$

4.3. Variable Order Inverse Fractional Fourier Reconstruction

Finally, the third approach is to use the actual locations where the data was acquired. To solve the variable order inverse problem we propose a discrete approach, which fits well with the discrete samples and can also provide a continuous reconstruction. Each sample

in ρ–α space (ρ_n, α_n) acquired at $t = t_n$ corresponds to one coefficient of the FrFT of order $a_n = 2\alpha_n/\pi$. These coefficients can be thought as the expansion of the object on the bases formed by the "chirp" functions. These functions are given by the inverse FrFT of order a_n of a delta function located at $\rho = \rho_n$ (Ozaktas et al., 2001):

$$\begin{aligned} \Delta_{-a_n}(u) &= \mathcal{F}^{-a_n}\left\{\delta(\rho - \rho_n)\right\}(u) \\ &= C^*_{\alpha_n}(\rho_n)\, e^{-i\pi(u^2 \cot\alpha_n - 2u\rho_n \csc\alpha_n)} \end{aligned}$$

where * denotes complex conjugate. Recalling that the samples (ignoring again the constant field shift, p_0) are defined by

$$f_{a_n}(\rho_n) = C_{\alpha_n}(\rho_n) s(t_n)$$

we have an estimation of the object as the weighted sum of all contributions.

$$\begin{aligned} \hat{f}_\alpha(u) &= \sum_{n=1}^{N} f_{a_n}(\rho_n)\Delta_{-a_n}(u) \\ &= \sum_{n=1}^{N} |\csc\alpha_n| s(t_n) e^{-i\pi(u^2\cot\alpha_n - 2u\rho_n\csc\alpha_n)} \end{aligned}$$

We assume a uniform sampling density, otherwise it would be necessary to incorporate a factor proportional to $\dot{\rho}(t_n)$ which arises from the underlying discretization of the inverse FrFT integral by Riemann sums.

The object $\hat{f}_\alpha(u)$ can be evaluated for any continuous value of u. Note that if we substitute α_n by $\pi/2$ this formula becomes the definition of the Discrete Frequency Fourier Transform (DFFT), or the Discrete Fourier Transform (DFT), if u is also evaluated at discrete values. If α_n is substituted by another fixed angle, other than $\pi/2$, the reconstruction is also the DFFT, but with an extra phase and an additional constant scaling factor. This is the discrete version of the inverse Fractional Fourier Transform.

The 2D extension of this reconstructions is:

$$\hat{f}(\mathbf{u}) = \sum_{n=1}^{N} |\det(\mathbf{B}_n)| s(t_n)\, \mathrm{e}^{-i\pi(\mathbf{u}^{\mathrm{T}}\mathbf{A}_n\mathbf{u} - 2\mathbf{u}^{\mathrm{T}}\mathbf{B}_n\boldsymbol{\rho}_n)} \tag{4.2}$$

4.4. Units

So far we have used ρ and u as dimensionless variables. To ensure the validity of the former analysis and extend it to practical cases, we use the normalization $u = x/q$ in which

$$f(u) = f(x/q) = \sqrt{q}\tilde{f}(x) \tag{4.3}$$

with $\tilde{f}(x)$ the dimensional object. The scale parameter q has the same dimension as x. In the discrete case, we need longitudes in ρ to be independent of α, which can be achieved by setting $q = FOV/\sqrt{N}$ (Koc, Ozaktas, Candan, & Kutay, 2008) where FOV is the field of view in distance units and N is the number of samples. This normalization is independently applied for each dimension.

5. EXPERIMENTS AND METHODS

All MRI images mentioned in this section were acquired in a Philips Intera 1.5T scanner. Linear shimming was disabled during all acquisitions and no higher order active shimming was used. The sequences were performed without any consideration about ρ–α space, using mostly default parameters from pre–loaded sequences in the system. Complex–valued image reconstructions were performed off–line.

5.1. Analytical phantom

In our first experiment, the MR signal for a two dimensional (2D) analytical magnetization phantom was simulated by numerically evaluating (3.1) using adaptive quadrature in MATLAB (Shampine, 2008), nesting a one–dimensional evaluation for each dimension. The phantom was designed as a simplified version of a real reference phantom with the same dimensions. The acquisition time of each sample and k–space locations were determined considering 2DFT gradients used in a standard Fourier acquisition. We simulated a cartesian matrix of 256 $\times$ 256 samples with a field of view (FOV) of 25.6 $\times$ 25.6 cm and echo time $\mathrm{TE} = 56$ ms. Each complete readout in the sequence takes 28 ms.

Two signals were simulated, the first with a uniform B_0 field and the second with a quadratic field. The quadratic deviation was chosen to emulate the measured quadratic component for a real phantom, but doubling its values to increase the effect of the distortion in the simulation, and at the same time keeping it within a valid physical range.

5.2. MRI phantom

In a second experiment, we scanned an MRI phantom using a fast field echo (FFE) echo–planar imaging (EPI) sequence, with a scan matrix of 128 $\times$ 128 samples, image FOV of 24 $\times$ 24 cm, slice thickness 5 mm, flip angle 23°, repetition time TR $=$ 650 ms and echo time TE $=$ 41 ms. This data was acquired with a number of sample averages (NSA) of 16 using a Q–body coil. The EPI factor in this sequence is 63. Each complete readout in this sequence took 76 ms.

5.3. *In–vivo* study

An *in–vivo* study was done scanning the brain of a volunteer, the images were acquired using the same sequence used for the phantom study, except from NSA which was now 8 and from the receiving coil which was now a standard quadrature head coil. A slightly angled transversal slice of the brain was selected.

5.4. Field maps

In each experiment, structural images were acquired with short readout time sequences to minimize the effect of field inhomogeneity. The magnetic field was measured in each location from phase differences in two images with different echo time, using $\Delta\omega(x, y) = \Delta\phi(x, y)/\Delta\text{TE}$ (Schneider & Glover, 1991) with a short ΔTE to avoid phase wrapping in the resulting field map.

To fit quadratic functions to the field maps, we used a maximum likelihood method that minimizes the weighted squared error between the measured field map and a parametric separable second order polynomial evaluated at corresponding positions. The weights were the mean of the corresponding pixels in the magnitude of the images from which the phase difference had been obtained. This ensures that the field map information was incorporated correctly depending on the local intensity of the signal and its signal to noise ratio. In the case of the *in–vivo* study, a region of interest was defined by setting to zero the weighting outside it.

In the phantom study, the field map was determined along a structural reference image using $\Delta\text{TE} = 3$ ms and TR and TE equal to 14 and 6.1 ms respectively. A transversal slice of the physical phantom was selected for this study.

For the *in–vivo* study, the structural reference image was obtained with TR and TE equal to 17 and 6.2 ms respectively for the same field of view and resolution. The field map was computed with $\Delta\text{TE} = 6$ ms. The anatomy causes further field deviations which cannot be approximated by the fitted function for the entire FOV. We therefore used an

elliptical region of interest (ROI) where the field is mainly quadratic and the approximation is suitable to demonstrate the proposed reconstruction.

Field maps and profiles displayed in all figures in Chapter 6 share the same color scaling, mapping the entire range to a 180 Hz difference, with the lowest and highest intensities mapped to -140 Hz and 40 Hz respectively. To display the measured field maps and phase images, the field map value was set to zero wherever the intensity of the signal was below 5% of its maximum value.

5.5. Image reconstruction

In all experiments, image reconstruction was performed by estimating the magnetization of the object computing (4.2) and evaluating $\mathbf{u}$ at the corresponding positions in dimensionless coordinates. Distance units of the results were scaled using (4.3) to map the estimated object into the dimensional coordinates. Three different reconstruction schemes were used in each experiment, producing three object estimations according to diagrams (a), (b) and (c) in Fig. 4.1. The first one is standard inverse Fourier (FT) reconstruction and used $\alpha_{un} = \alpha_{vn} = \pi/2,\ \forall n = 1 \ldots N$. The second one, inverse fractional Fourier (FrFT) reconstruction, used $\alpha_{un} = \bar{\alpha_u}, \alpha_{vn} = \bar{\alpha_v},\ \forall n = 1 \ldots N$ with $\bar{\alpha_u}$ and $\bar{\alpha_v}$ equal to the angles at the origin of the four–dimensional ρ–α space during the readout. Variable order inverse fractional Fourier (VO–FrFT) reconstruction took into account the exact position in ρ–α space of each sample.

6. RESULTS

6.1. Analytical phantom

One can observe the distortions produced by a quadratic field when using the standard Fourier reconstruction, by comparing Figures 6.1 (a) and (b). We appreciate a geometric distortion, characteristic of data acquired under field inhomogeneity, which is proportional to the local field deviation from the central frequency. The phase of the reconstructed image has a complex quadratic modulation although the analytical phantom did not have phase. An intensity nonuniformity distortion is also noted, in which the distorted image

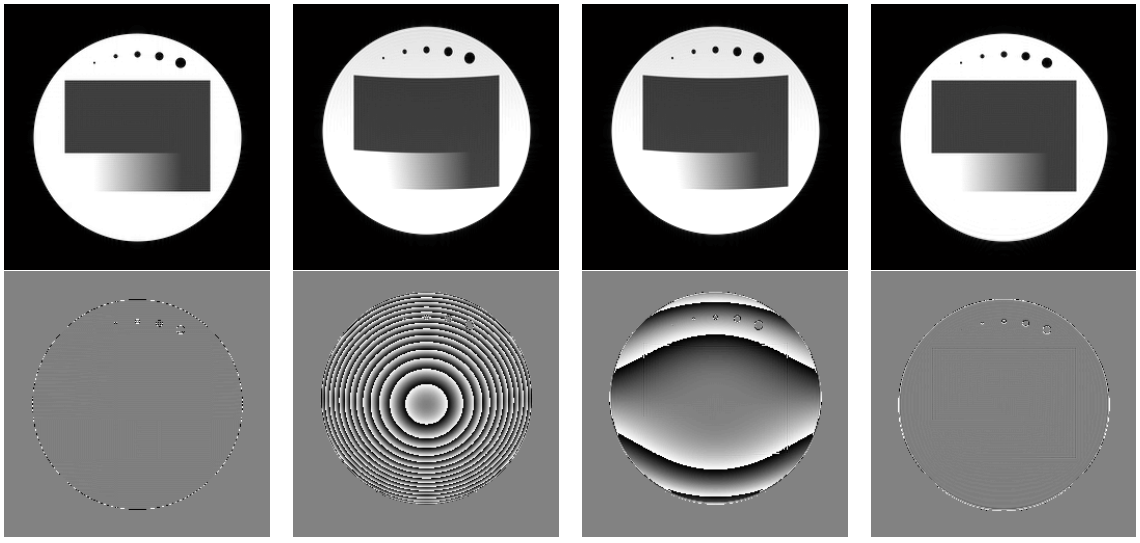

(a) (b) (c) (d)

FIGURE 6.1. Reconstruction results for 2DFT simulations with an isotropic quadratic field. Each column shows magnitude and phase images with the same color scaling. Magnitude and phase move from 0 to 1 and from $-\pi$ to π respectively. Phase values have been set to zero when magnitude is below 5% of maximum. (a) Ideal reconstruction for a homogeneous field simulation and standard inverse Fourier reconstruction. The remaining columns show reconstructions for a quadratic field simulation. (b) Standard inverse Fourier reconstruction. (c) Inverse fractional Fourier reconstruction with constant α approximation for each echo. (d) Variable order inverse fractional Fourier reconstruction considering exact trajectory.

has an intensity approximately 12% lower in the upper section of the object and a simmilar inverse variation in the lower section.

As expected by means of (4.1), the reconstruction result for inverse fractional Fourier (FrFT) reconstruction (Fig. 6.1 (c)) shows identical magnitude than the standard inverse Fourier (FT) reconstruction (Fig. 6.1 (b)) but with a phase much closer to the actual phase. The variable order inverse fractional Fourier (VO–FrFT) reconstruction corrected the image distortions in magnitude and phase, including the geometric distortion (Fig. 6.1 (d)).

6.2. MRI phantom

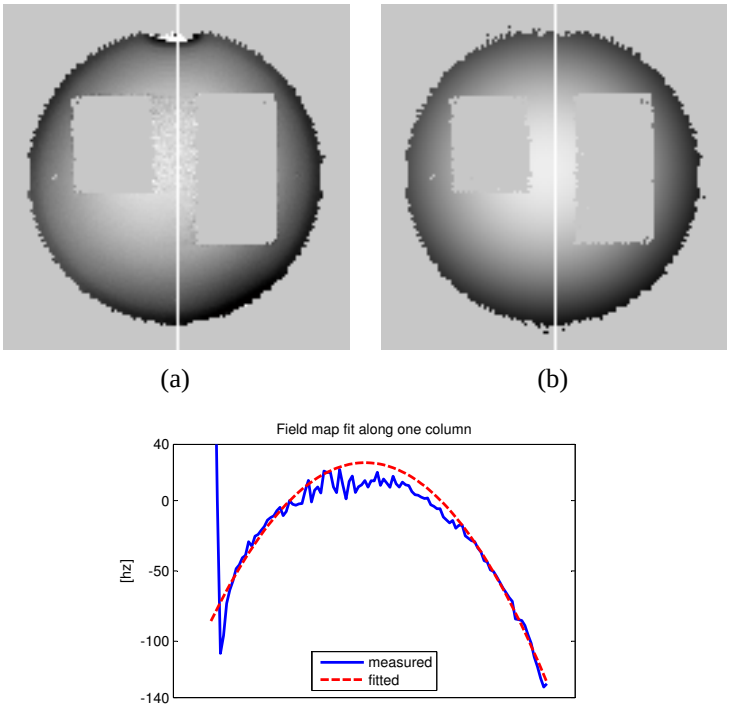

FIGURE 6.2. Field map fit for MRI Phantom. (a) Measured field map. (b) Fitted field map. (c) Along the marked column, the measured magnetic field (solid line) can be approximated by a quadratic function (dashed line).

In the MRI phantom study, we have found that the particular combination of our MR system with its intrinsic inhomogeneity and the scanned phantom produced a field map

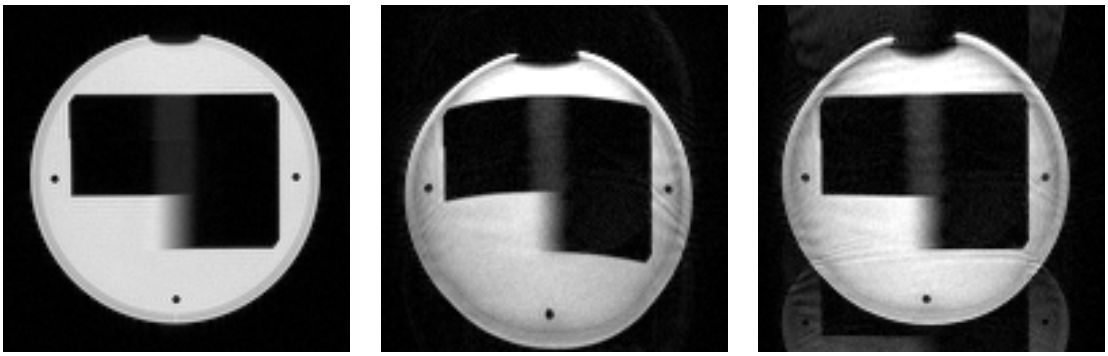

(a) (b) (c)

FIGURE 6.3. Reconstruction results for MRI Phantom under a quadratic field. Geometric distortions shown in (b) obtained using standard inverse Fourier reconstruction can be corrected in (c) using variable order inverse fractional Fourier reconstruction, compared to a low distortion image (a).

that resembles an isotropic quadratic function with its highest intensity in the center of the magnet as shown in Fig. 6.2.

In this study, the phase information of the object is unknown since we cannot acquire it with the same contrast as the distorted object but without the effect of the quadratic field map. We will compare the magnitude of the reconstructions of the distorted signal with the magnitude of a low distortion image acquired with short readouts.

The FT reconstruction shown in Fig. 6.3 (b) produces geometric and intensity distortions similar to those observed in the simulation study for a quadratic field (Fig. 6.1 (b)). Figure 6.3 also shows that the VO–FrFT reconstruction (c), partially corrects these distortions, improving the geometry and intensity of the estimation when comparing both reconstructions against the low distortion image (a). Ghosting artifacts are visible in (c) which we do not fully understand, but we believe to be related to an incomplete phase correction typically used to reduce the EPI ghosting artifact.

As expected, magnitudes of the fractional Fourier reconstruction and standard Fourier reconstruction were identical, therefore the first one was omitted from the figures.

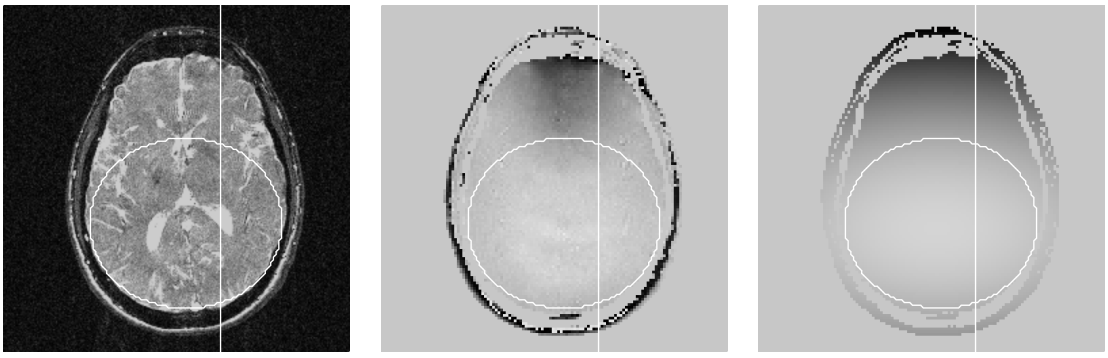

(a) (b) (c)

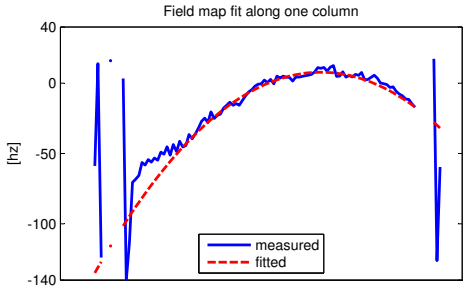

(d)

FIGURE 6.4. Field map fit for *in–vivo* study. (b) Measured field map. (c) Fitted field map. Within the elliptical ROI in (a), the measured magnetic field can be approximated by a quadratic function as shown in (d) with solid and dashed lines respectively for the marked column.

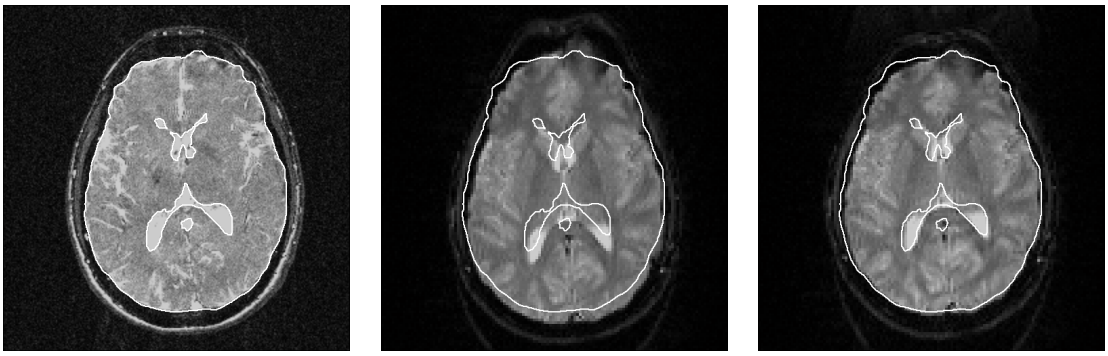

(a) (b) (c)

FIGURE 6.5. Reconstruction results for *in–vivo* study. The superimposed contours show the location of some key features in the reference image (a). (b) Standard inverse Fourier reconstruction. (c) Variable order inverse Fourier reconstruction with corrected quadratic field inhomogeneity.

6.3. *In–vivo* study

With the volunteer experiment we found the magnetic field to vary smoothly inside the brain. In particular, the field can be approximated by a quadratic function within an elliptical region of interest (ROI) as shown in Fig. 6.4. The VO–FrFT reconstruction partially corrects most of the geometric distortions present in the FT reconstruction as can be seen in Fig. 6.5, especially in the regions in which the fitted quadratic function is a close approximation of the field map. To facilitate the comparison we have superimposed on all reconstructions in Fig. 6.5 contours that show the actual location of key features taken from the reference image (a).

7. CONCLUSIONS

Traditionally, MRI reconstruction is performed applying an inverse Fourier Transform (FT) of the acquired MR signal. This method rests on the base that the object has been magnetized with a perfectly uniform magnetic field. In practice, it is not possible to get a uniform field because of physical restrictions and susceptibility variations at the scanned object. This is a critical problem as the MR community is pushing for getting short–bore and high–field MR systems, which are exactly the kind of factors that tend to increase field inhomogeneities. Additionally, sequences with long acquisition windows, such as EPI and spiral, are increasingly used. These sequences are severely affected by inhomogeneity–related artifacts. Modern MR systems always include linear field corrections and higher-order polynomial field corrections are getting a common feature. It is therefore reasonable to think that main magnetic fields are not intrinsically uniform. In fact, in all our experiments our magnet showed a nearly quadratic behavior.

We present a new, strongly supported framework for quadratic inhomogeneity MR signal analysis based on the Fractional Fourier Transform (FrFT). It restores the theoretical relation between image space and quadratic magnetic field signal space, allowing native second order field image reconstruction (or correction). The FrFT transform, which is a generalization of the FT, has a quadratic term in its integral kernel, so that there is a natural link between the signal obtained from an object magnetized with a quadratic field and its FrFT. This new framework and the ρ–α space we introduce give a visual insight to the MR acquisition process and also, provide a meaningful graphical representation that shows the relation between the image domain, the standard k–space and FrFT domains.

Our experiments showed that our proposed method, the variable order fractional Fourier reconstruction (VO–FrFT), can effectively reconstruct MRI signals under nearly quadratic magnetic fields, without being affected by the geometric distortions that appear when those signals are reconstructed by the standard FT scheme.

One effect of analyzing MR data using ρ–α space is that k is scaled down by a factor $\csc\alpha \geq 1$. This scaling is not homogeneous in k–space but depends on the time map of

the sequence. For a given sequence planned for ordinary k–space acquisition, this fact is manifested as a resolution loss. These resolution losses could be reduced using stronger gradients with an ordinary sequence or modifying the sequence to fill ρ–α space at corrected locations.

New trajectories should be designed to fill ρ–α space in order to meet image resolution requirements. Theoretical advances are also needed to replace the Nyquist sampling rate for k–space with a similar criterion which would indicate how information density is distributed along ρ–α space.

Our approach based on the Fractional Fourier Transform gives a new theoretical MR framework between image space and signal space for quadratic field MR systems, allowing native image reconstruction for second order main fields. Hopefully, this new approach will reduce the hardware complexity of MR systems, since the second order terms in the main magnetic field would no longer be a concern.

REFERENCES

Akel, J. A., Rosenblitt, M., & Irarrazaval, P. (2002, Feb). Off-resonance correction using an estimated linear time map. *Magnetic resonance imaging*, *20*(2), 189-198.

Bultheel, A. (2004). Computation of the fractional fourier transform. *Applied and Computational Harmonic Analysis*, *16*(3), 182.

Candan, C., Kutay, M. A., & Ozaktas, H. M. (2000). The discrete fractional fourier transform. *IEEE Transactions on Signal Processing*, *48*(5), 1329.

Chen, W., & Meyer, C. H. (2008, May). Semiautomatic off-resonance correction in spiral imaging. *Magnetic Resonance in Medicine*, *59*(5), 1212-1219.

Chen, W., Sica, C. T., & Meyer, C. H. (2008, Nov). Fast conjugate phase image reconstruction based on a chebyshev approximation to correct for b0 field inhomogeneity and concomitant gradients. *Magnetic Resonance in Medicine*, *60*(5), 1104-1111.

Fessler, J. A., Lee, S., Olafsson, V. T., Shi, H. R., & Noll, D. C. (2005). Toeplitz-based iterative image reconstruction for mri with correction for magnetic field inhomogeneity. *IEEE Transactions on Signal Processing*, *53*(9), 3393-3402.

Guven, H. E., Ozaktas, H. M., Cetin, A. E., & Barshan, B. (2008). Signal recovery from partial fractional fourier domain information and its applications. *IET Signal Processing*, *2*(1), 15.

Irarrazabal, P., Meyer, C. H., Nishimura, D. G., & Macovski, A. (1996, Feb). Inhomogeneity correction using an estimated linear field map. *Magnetic Resonance in Medicine*, *35*(2), 278-282.

Kalinowski, H., Berger, S., & Braun, S. (1988). *Carbon-13 nmr spectroscopy*. Chichester: Wiley.

Koc, A., Ozaktas, H. M., Candan, C., & Kutay, M. A. (2008). Digital computation of linear canonical transforms. *IEEE Transactions on Signal Processing*, *56*(6), 2383-2394.

Liang, Z., & Lauterbur, P. C. (2000). *Principles of magnetic resonance imaging: a signal processing perspective*. Bellingham, Washington: SPIE Optical Engineering Press.

Manjón, J. V., Lull, J. J., Carbonell-Caballero, J., García-Martí, G., Martí-Bonmatí, L., & Robles, M. (2007, 8). A nonparametric mri inhomogeneity correction method. *Medical image analysis*, *11*(4), 336-345.

Noll, D. C., Fessler, J. A., & Sutton, B. P. (2005). Conjugate phase mri reconstruction with spatially variant sample density correction. *IEEE Transactions on Medical Imaging*, *24*(3), 325-336.

Ozaktas, H. M., Arikan, O., Kutay, M. A., & Bozdagt, G. (1996). Digital computation of the fractional fourier transform. *IEEE Transactions on Signal Processing*, *44*(9), 2141.

Ozaktas, H. M., Barshan, B., & Mendlovic, D. (1994). *Convolution and filtering in fractional fourier domains.*

Ozaktas, H. M., Barshan, B., Mendlovic, D., & Onural, L. (1994). Convolution, filtering, and multiplexing in fractional fourier domains and their relation to chirp and wavelet transforms. *Journal of the Optical Society of America A*, *11*(2), 547.

Ozaktas, H. M., Kutay, M. A., & Zalevsky, Z. (2001). *The fractional fourier transform with applications in optics and signal processing*. Chichester, New York: Wiley.

Ozaktas, H. M., & Mendlovic, D. (1993). Fourier transforms of fractional order and their optical interpretation. *Optics Communications*, *101*(3-4), 163-169.

Ozaktas, H. M., & Mendlovic, D. (1995). Fractional fourier optics. *Journal of the Optical Society of America A*, *12*(4), 743.

Ozaktas, H. M., & Sumbul, U. (2006). Interpolating between periodicity and discreteness through the fractional fourier transform. *IEEE Transactions on Signal Processing*, *54*(11), 4233-4243.

Schneider, E., & Glover, G. (1991, Apr). Rapid in vivo proton shimming. *Magnetic Resonance in Medicine*, *18*(2), 335-347.

Shampine, L. F. (2008). Vectorized adaptive quadrature in matlab. *Journal of Computational and Applied Mathematics*, *211*(2), 131-140.

Sutton, B. P., Noll, D. C., & Fessler, J. A. (2003). Fast, iterative image reconstruction for mri in the presence of field inhomogeneities. *IEEE Transactions on Medical Imaging*, *22*(2), 178-188.

Vaughan, T., DelaBarre, L., Snyder, C., Tian, J., Akgun, C., Shrivastava, D., et al. (2006, Dec). 9.4t human mri: preliminary results. *Magnetic Resonance in Medicine*, *56*(6), 1274-1282.

Vedrine, P. (2008). The whole body 11.7 t mri magnet for iseult/inumac project. *IEEE Transactions on Applied Superconductivity*, *18*(2), 868.

Vovk, U., Pernus, F., & Likar, B. (2004, Sep 7). Mri intensity inhomogeneity correction by combining intensity and spatial information. *Physics in Medicine and Biology*, *49*(17), 4119-4133.

Yetik, I. S. (2001). Image representation and compression with the fractional fourier transform. *Optics Communications*, *197*(4-6), 275.